Broadband Absorption Spectroscopy via Excitation of Lossy Resonance Modes in Thin Films

D. Razansky,[1,*] P. D. Einziger,[2] and D. R. Adam[1]

[1]Department of Biomedical Engineering, Technion–Israel Institute of Technology, Haifa 32000, Israel
[2]Department of Electrical Engineering, Technion–Israel Institute of Technology, Haifa 32000, Israel

(Received 12 February 2005; published 30 June 2005)

It is shown that broadband absorption spectroscopy utilizing thin lossy film configurations can be optimally facilitated when applied to metallic and insulating materials. For metallic films, the zero-order highly lossy resonance mode, characterized by ultra wideband absorption behavior under normal incidence, can be shifted, under parallel-polarization oblique incidence, toward a narrow band light-wavelength surface plasmon resonance condition. Higher order low-loss modes, however, occur in thin insulating films, exhibiting Debye relaxation behavior, typical for many aqueous solutions and biological substances. They can be excited in a highly scalable and sensitive manner in various frequency bands, between light and radio frequencies.

DOI: 10.1103/PhysRevLett.95.018101 PACS numbers: 87.64.−t, 73.20.Mf, 77.55.+f, 79.60.Dp

Thin dissipative films are widely utilized in various microscopy and spectroscopy methods for characterization of surface and bulk physical properties of materials (e.g., [1–3]). In general, high quality factor resonances cannot be easily obtained in the presence of material losses, which play a crucial role in establishing highly sensitive and robust refractive index measurements for these methods. Herein, the recently presented optimal absorption paths approach for normal incidence symmetrical case [4], is extended to incorporate oblique incidence of electromagnetic waves upon asymmetrically surrounded lossy film, allowing an effective implementation in a novel absorption spectroscopy method. Rigorous solution of macroscopic Maxwell equations in a thin film limit renders a closed-form prediction of all possible lossy resonance modes (LRM) and their universal absorptivity bound. The zero-order LRM reveal and define the conditions for the well-known surface plasmon resonance (SPR) total absorption, known as one of the most sensitive subwavelength spectroscopy technique and widely utilized for monitoring hybridization reactions, biomolecule and chemical sensing, characterization of ultrathin films adsorbed onto noble metal surfaces, as well as being currently explored for its potential in subwavelength optics and data storage [2,5–7]. Being limited to near-plasma frequencies of metals, lying in the visible and near-infrared bands, surface plasmons can be excited under very specific conditions and usually have poor penetration depth into adsorbing layers [8]. Nevertheless, it is demonstrated here that ultrasensitive and highly scalable refractive index absorption spectroscopy is possible for a wide range of frequency bands, from rf (radio frequency) to submillimeter and light wavelengths, using excitation of high-order (Fabry-Perot-type) LRM in thin insulating films.

Assuming a harmonic time dependence $e^{-i\omega t}$ of the obliquely incident plane wave (Fig. 1), the corresponding wave numbers $k_1 = \omega\sqrt{\varepsilon_1\mu_1}$, $k_2 = \omega\sqrt{\varepsilon_2\mu_2}$, and $k_3 = \omega\sqrt{\varepsilon_3\mu_3}$ satisfy $\Im\{k_1\}, \Im\{k_2\}, \Im\{k_3\} \geq 0$, respectively. Similarly, the normalized (generally complex) refractive indexes $n_{21} = k_2/k_1$, $n_{32} = k_3/k_2$, and $n_{31} = k_3/k_1$ and the corresponding normalized permeabilities $\mu_{21} = \mu_2/\mu_1$, $\mu_{32} = \mu_3/\mu_2$, and $\mu_{31} = \mu_3/\mu_1$ are introduced. The global reflection and transmission coefficients of the film, for the transversial electric field components, are well known (e.g., [9]) and can be represented via

$$R = \frac{r_{12} + r_{23}e^{2ik_2 d\cos\theta_2}}{1 + r_{12}r_{23}e^{2ik_2 d\cos\theta_2}} = -\frac{\sin[(\psi_{12} - \psi_{23})/2 - \varphi]}{\sin[(\psi_{12} + \psi_{23})/2 + \varphi]} \quad (1)$$

and

$$T = \frac{(1 + r_{12})(1 + r_{23})e^{ik_2 d\cos\theta_2}}{1 + r_{12}r_{23}e^{2ik_2 d\cos\theta_2}} = \frac{t_{13}\sin[(\psi_{12} + \psi_{23})/2]}{\sin[(\psi_{12} + \psi_{23})/2 + \varphi]}, \quad (2)$$

respectively, where the intrinsic reflection and transmission coefficients r_{12}, r_{23}, t_{13}, and phases ψ_{12} and ψ_{23} are defined in Table I. Subsequently, φ in (1) and (2) is defined via

$$\varphi = k_2 d\cos\theta_2 = \delta_{\mathrm{TM}}^{\mathrm{TE}}\mathcal{Z}_{12}^{\mathrm{TM}}\cos_2^0\theta_2, \quad \delta_{\mathrm{TM}}^{\mathrm{TE}} = k_1 d\mu_{21}\cos^{\pm 1}\theta_1, \quad (3)$$

or, explicitly, via Snell's law (Fig. 1) and Table I, by

$$\varphi = \frac{i\delta_{\mathrm{TM}}^{\mathrm{TE}}2_{-1}^{0}}{\tan(\psi_{12}^{\mathrm{TM}}/2)}\left[1 + \sqrt{1 + \left[\tan\left(\frac{\psi_{12}^{\mathrm{TM}}}{2}\right)\frac{\sin(2\theta_1)}{\mu_{21}}\right]^2}\right]_1^0. \quad (4)$$

The distinguishing superscripts $^{\mathrm{TE}}$ and $^{\mathrm{TM}}$, corresponding

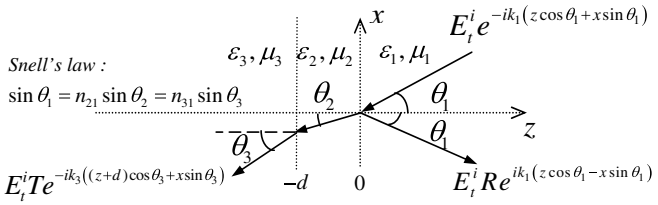

FIG. 1. Physical configuration: oblique incidence of plane monochromatic wave upon thin absorbing film.

to the two elementary plane-wave polarizations, have been partially omitted in Eqs. (1)–(4) and Table I, only for relations applying to both polarizations. This rule is adapted throughout the Letter for all the equations that apply to both polarizations. The fraction of the incident wave's power, absorbed in the film, i.e., the power absorption efficiency, is thus given via

$$\eta = 1 - |R|^2 - |T|^2 \Re\{\mathcal{Z}_{13}\}. \tag{5}$$

The optimal power absorption condition for the normalized impedance $\mathcal{Z}_{12}$ of the layer (and, subsequently, for n_{21}), depending parametrically on its normalized thickness δ and on the normalized impedance $\mathcal{Z}_{13}$ of the two surrounding layers, can be readily obtained via optimization of η with respect to ψ_{12}, i.e.,

$$\frac{d\eta}{d\psi_{12}} = \frac{\partial\eta}{\partial\psi_{12}} + \frac{d\psi_{23}}{d\psi_{12}}\frac{\partial\eta}{\partial\psi_{23}} + \frac{d\varphi}{d\psi_{12}}\frac{\partial\eta}{\partial\varphi} = 0. \tag{6}$$

Utilizing (5) and the explicit expressions for $d\varphi/d\psi_{12}$ and $d\psi_{23}/d\psi_{12}$ (Table I) in conjunction with (6) leads to an implicit equation for optimal $\psi_{12,\mathrm{opt}}$, $\psi_{23,\mathrm{opt}}$, and φ_{opt}, i.e.,

$$\begin{aligned}|t_{13}|^2\Re\{\mathcal{Z}_{13}\}\sin\left(\frac{\psi_{12}^* + \psi_{23}^*}{2}\right)&\left\{\left(1 + \frac{d\psi_{23}}{d\psi_{12}}\right)\sin\varphi\right.\\ &\left. - 2\frac{d\varphi}{d\psi_{12}}\sin\left(\frac{\psi_{12} + \psi_{23}}{2}\right)\cos\left(\frac{\psi_{12} + \psi_{23}}{2} + \varphi\right)\right\}\\ &= \left[\left(\frac{d\psi_{23}}{d\psi_{12}} + 2\frac{d\varphi}{d\psi_{12}}\right)\sin\psi_{12} - \sin(\psi_{23} + 2\varphi)\right]\\ &\quad\times\sin\left(\frac{\psi_{12}^* - \psi_{23}^*}{2} - \varphi^*\right),\end{aligned} \tag{7}$$

where x^* denotes complex conjugate of x. In the thin film limit, i.e., when the normalized thickness $\delta \to 0$, if also $\varphi \sim \delta\mathcal{Z}_{12} \to 0$, then [via (1) and (2) and Table I]: $R|_{\varphi\to 0} = r_{13}$, $T|_{\varphi\to 0} = t_{13}$, leading to $\eta|_{\delta,\varphi\to 0} = 0$. Thus, in this asymptotic limit, higher efficiency can be obtained only if $\mathcal{Z}_{12}$ is unbounded, i.e., $\psi_{12} \sim 2i/\mathcal{Z}_{12} \to 0$. Moreover, $\psi_{12} \to 0$ leads to $\psi_{23} \to 0$. Noting that $\tan x \sim \sin x \sim x$ and $\cos x \sim 1$, as $x \to 0$, results in (via Table I) $\psi_{23} \sim \psi_{12}\mathcal{Z}_{13}$, $d\psi_{23}/d\psi_{12} \sim \mathcal{Z}_{13}$, and $d\varphi/d\psi_{12} \sim -\varphi/\psi_{12}$, leading to the following thin film approximation of (7), containing terms up to $O(\psi_{12})$, i.e.,

$$\begin{aligned}\Re\{\mathcal{Z}_{13}\}\psi_{12,\mathrm{opt}}^*\cos((1 + \mathcal{Z}_{13})\psi_{12,\mathrm{opt}}/2 + \varphi_{\mathrm{opt}})&\\ = \sin(\varphi_{\mathrm{opt}}^* - (1 - \mathcal{Z}_{13}^*)\psi_{12,\mathrm{opt}}^*/2).&\end{aligned} \tag{8}$$

Since $\psi_{12,\mathrm{opt}} \to 0$ and, thus, $\psi_{12,\mathrm{opt}}^* \to 0$, Eq. (8) can be fulfilled for

$$\varphi_{\mathrm{opt}} \sim (1 + \mathcal{Z}_{13}^*)\psi_{12,\mathrm{opt}}/2 + m\pi \sim 2i\delta/\psi_{12,\mathrm{opt}}, \tag{9}$$

where $m = 0, 1, 2, \ldots$. Solving the quadratic equation for $\psi_{12,\mathrm{opt}}$ in (9) and subsequently expressing $\mathcal{Z}_{12} \sim \varphi_{\mathrm{opt}}/\delta$ via ψ_{12} in (9), renders a closed-form asymptotic expression for an infinite number of LRM,

$$\mathcal{Z}_{12,\mathrm{opt},m} \sim \frac{\pi m}{2\delta}\left[1 + \sqrt{1 + \frac{i4[1 + \mathcal{Z}_{13}^*]\delta}{(\pi m)^2}}\right]. \tag{10}$$

Substitution of $m = 0$ provides the following approximation for the zero-order LRM, i.e.,

$$\mathcal{Z}_{12,\mathrm{opt},0} \sim (1 + i)\sqrt{(1 + \mathcal{Z}_{13}^*)/(2\delta)}. \tag{11}$$

High-order LRM are obtained for either $\delta \ll 1$ or $m \gg 1$ as

$$\mathcal{Z}_{12,\mathrm{opt},m} \sim \pi m/\delta + i(1 + \mathcal{Z}_{13}^*)/(\pi m). \tag{12}$$

It should be noted that, in the limit of a thin film, the normalized impedance $\mathcal{Z}_{12}$ can be asymptotically translated (via Table I) into the normalized complex refractive index n_{21} as

$$n_{21,\mathrm{opt},m} \sim \mathcal{Z}_{12,\mathrm{opt},m}^{\mathrm{TE}_{\mathrm{TM}}}\mu_{21}\cos^{\pm 1}\theta_1. \tag{13}$$

Finally, substituting the asymptotic results for $\psi_{1,\mathrm{opt}}$, $\psi_{2,\mathrm{opt}}$, and φ_{opt} into (5) renders the following universal asymptotic value of the optimal power absorption efficiency in the thin film limit, valid, simultaneously, for all the lossy resonance modes, namely,

$$\eta_{\mathrm{opt}} \sim 1/(1 + \Re\{\mathcal{Z}_{13}\}), \qquad m = 0, 1, 2, \ldots. \tag{14}$$

Power absorption efficiency of thin films is thus asymptotically bounded by (14) for any selection of $\mathcal{Z}_{12}$, depending on $\Re\{\mathcal{Z}_{13}\}$ only, i.e., on the wave impedances of the surrounding media n_{31}/μ_{31} and the incidence angle θ_1 of the plane wave. It is readily reduced to $\eta_{\mathrm{opt}} \sim 1/2$ for the normal incidence symmetrical case [4], having $\mathcal{Z}_{13} = 1$. Above the critical angle $\theta_1 > \theta_{1,c} = \sin^{-1} n_{31}$, however, for which $\Re\{\mathcal{Z}_{13}\} = 0$ (assuming $\Im\{n_{31}\} = 0$), η_{opt} in (14) attains its maximum, namely $\eta_{\mathrm{opt}} = 1$, regardless of the imaginary part of $\mathcal{Z}_{13}$.

The optimal normalized impedance $\mathcal{Z}_{12,\mathrm{opt}}$, obtained implicitly via (7) or asymptotically via (10)–(12), charac-

TABLE I. Normalized intrinsic reflection and transmission coefficients, the associated impedances, and phase relations.

Normalized intrinsic reflection and transmission coefficients	Normalized impedances	Phase relations
$r_{12} = \frac{1-\mathcal{Z}_{12}}{1+\mathcal{Z}_{12}} = -e^{i\psi_{12}}$	$\mathcal{Z}_{12}^{\mathrm{TE}_{\mathrm{TM}}} = \frac{n_{21}}{\mu_{21}}\left(\frac{\cos\theta_2}{\cos\theta_1}\right)^{\pm 1}$	$\tan\left(\frac{\psi_{12}}{2}\right) = \tan\left(\frac{\psi_{23}}{2}\right)/\mathcal{Z}_{13} = \frac{i}{\mathcal{Z}_{12}}$
$r_{23} = \frac{1-\mathcal{Z}_{23}}{1+\mathcal{Z}_{23}} = e^{i\psi_{23}}$	$\mathcal{Z}_{23} = \frac{\mathcal{Z}_{13}}{\mathcal{Z}_{12}}$	$\frac{d\psi_{23}}{d\psi_{12}} = \mathcal{Z}_{13}\frac{\cos^2(\psi_{23}/2)}{\cos^2(\psi_{12}/2)}$
$t_{13} = r_{13} + 1 = \frac{2}{1+\mathcal{Z}_{13}}$	$\mathcal{Z}_{13}^{\mathrm{TE}_{\mathrm{TM}}} = \frac{n_{31}}{\mu_{31}}\left(\frac{\cos\theta_3}{\cos\theta_1}\right)^{\pm 1}$	$\left(\frac{d\varphi}{d\psi_{12}}\right)^{\mathrm{TE}_{\mathrm{TM}}} = \mp\frac{\varphi}{\sin\psi_{12}^{\mathrm{TE}_{\mathrm{TM}}}}\left[1 + \frac{i2\varphi\tan(\psi_{12}^{\mathrm{TE}_{\mathrm{TM}}}/2)}{\delta^{\mathrm{TE}_{\mathrm{TM}}}}\right]^{0}_{-1}$

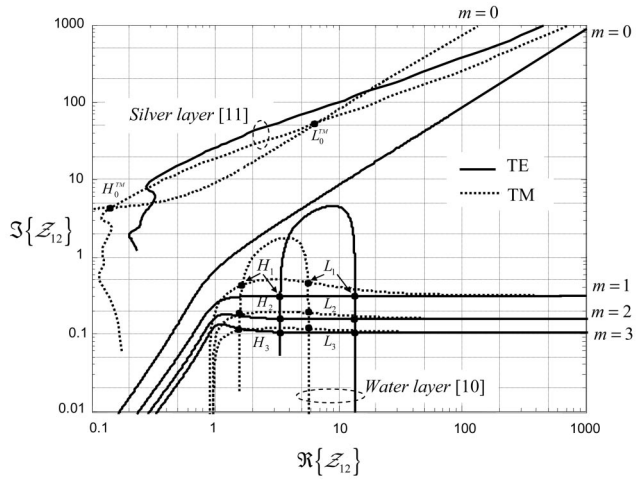

FIG. 2. Intersections of the first four optimal power absorption paths ($m = 0, 1, 2, 3$), obtained via (7), with the material (water and silver layers) dispersion curves in the complex $\mathcal{Z}_{12}$ domain. Oblique incidence above critical angle $\theta_1 = 50° > 49.5° = \theta_{1,c}$ for $n_{31} = 0.76$, $n_{10} = 1.33$, $\mathcal{Z}_{13}^{\mathrm{TE}} = 0.14i$, $\mathcal{Z}_{13}^{\mathrm{TM}} = -4i$, $\mu_{31} = \mu_{21} = 1$.

terizes two basic types of materials suitable for obtaining an optimally absorbing thin film of normalized width $\delta \ll 1$. This can be readily verified via the asymptotic expressions (12) and (11), associated with low-loss (insulating) and high-loss (metallic) type films, respectively. The solutions for $m \geq 1$ in (12), corresponding to the low-loss (Fabry-Perot-type) optimal LRM, exhibit the same dispersion behavior below and above the critical angle, since the dominant term of $O(1/\delta)$ in (12) is independent of $\mathcal{Z}_{13}$. Moreover, the same asymptotic expression (12) is valid for both TE and TM polarizations. This, however, is not the case for the $m = 0$ mode in (11). Below the critical angle, it matches, over ultrawide bands of frequencies and for both polarizations, the low-frequency dispersion relation of good conductors [4], characterized by the loss angle $\arg\{\mathcal{Z}_{12,\mathrm{opt}}\} = 45°$ in (11). Above the critical angle $\mathcal{Z}_{13}$ becomes purely imaginary (assuming that n_{31} is real), thus the loss angle can be shifted from the value of 45° by assigning imaginary values for $\mathcal{Z}_{13}$ in (11). As the incident angle varies in the range $\theta_{1,c} < \theta_1 < \pi/2$, the loss angle of $\mathcal{Z}_{12,\mathrm{opt}}$ for TE and TM polarized waves vary in the range $45° > \arg\{\mathcal{Z}_{12,\mathrm{opt}}^{\mathrm{TE}}\} > 0°$ and $90° > \arg\{\mathcal{Z}_{12,\mathrm{opt}}^{\mathrm{TM}}\} > 45°$, respectively, since above the critical angle $\Im\{\mathcal{Z}^{*\mathrm{TE}}{}_{13}\} > 0$ and $\Im\{\mathcal{Z}^{*\mathrm{TM}}{}_{13}\} < 0$. It is readily noted that, in the transition $\theta_{1,c} < \theta_1 < \pi/2$, the appropriate TE polarized optimal film varies from good electric conductor to poorly conducting material. As for the TM polarized optimal film, its dispersion behavior is, for $\theta_1 \approx \theta_{1,c}$, that of metals in the near-plasma frequency band and it becomes that of good electric conductors as $\theta_1 \to \pi/2$.

Experimental verification of the proposed optimization scheme for the near-plasma frequency band is obtained via [5], where the corresponding setup parameters $d = 40$ nm, $\lambda = 1152$ nm, $\theta_1 = 52.4°$, and $n_{31} = 1.322/1.7$ lead to $\mathcal{Z}_{13}^{\mathrm{TM}} = -2.434i$ and $\delta = 0.608$. Substituting into (7) via Table I renders $\mathcal{Z}_{12,\mathrm{opt}}^{\mathrm{TM}} = 0.116 + 2.596i$, i.e., $n_{21,\mathrm{opt}} = 0.187 + 4.327i$, and $\eta_{\mathrm{opt}} = 1$ in (5). This exact optimal result is in a very good agreement with the gold film data $n_{21}|_{\lambda=1152\,\mathrm{nm}} = (0.33 + 7.93i)/1.7 = 0.194 + 4.665i$ ([5], Table I) and the measured efficiency $\eta = 1 - |R|^2 \approx 0.99$ ([5], Fig. 1).

Once the frequency dispersion characteristics $n_{21}(\omega)$ and thickness d of a specific film, translated into $\mathcal{Z}_{12}$ and δ via Table I, match the optimal solution $\mathcal{Z}_{12,\mathrm{opt}}$, given implicitly in (7) or asymptotically in (11) and (12), a highly sensitive spectroscopy can be implemented. This is further demonstrated in Fig. 2 for water [10] and silver [11] layers, representing insulating (Debye) and metallic (Drude) type dispersions, respectively. One notes that the frequency dependent water dispersion curve intersects indeed with the optimal absorption high-order $m \geq 1$ paths (exact solutions of (6) or (7) for $\mathcal{Z}_{12,\mathrm{opt}}$ versus δ with a specified $\mathcal{Z}_{13}$) in the complex $\mathcal{Z}_{12}$ domain for both TE and TM polarizations, as expected. However, only the $m = 0$ path, corresponding to TM polarization, is intersected by the TM dispersion curve of silver in its high-frequency plasma band, resulting in the well-known SPR total absorption phenomenon [5,8]. The intersection between the TE dispersion curve for silver and the $m = 0$ TE path never occurs since the latter belongs to a good conductor region in the complex $\mathcal{Z}_{12}$ domain rather than the plasma region. The intersection points depicted in Fig. 2 for both silver and water are most conveniently divided into low-frequency ($L_0, \ldots, L_3$) and high-frequency ($H_0, \ldots, H_3$) intersection subsets.

The intersections in Fig. 2 can be generalized for any metallic or insulating material, upon utilizing their explicit dispersion relations, given via Drude and Debye formulas, respectively [10], as summarized in Table II. The optimal values in Table II were obtained by analytically determining the intersections between the dispersion formulas and the asymptotic expressions in (11) and (12). It should be

TABLE II. Asymptotic values of the optimal absorption resonant frequencies ω_{opt} and film thicknesses d_{opt} at intersections of material dispersion relations with optimal absorption paths in the normalized complex impedance domain $\mathcal{Z}_{12}$. The constants c, ε_{10}, and μ_{10} denote speed of light in vacuum and relative permittivity and permeability of the first (k_1) layer, respectively.

Dispersion relation [10], $n_{21}(\omega)$	Low-frequency intersections, Drude & Eq. (11), Debye & Eq. (12)	High-frequency intersections, Drude & Eq. (15), Debye & Eq. (12)
Drude-type: $\sqrt{\frac{\mu_{21}}{\varepsilon_{10}}\left(1 - \frac{\omega_p^2}{\omega^2 + i\omega\gamma}\right)}$	$\omega_{\mathrm{opt}}^{\mathrm{TM}} = \frac{\gamma\Im\{\mathcal{Z}_{13}^{*\mathrm{TM}}\}}{1+\Re\{\mathcal{Z}_{13}^{\mathrm{TM}}\}}$ $d_{\mathrm{opt}}^{\mathrm{TM}} = \frac{\lvert 1+\mathcal{Z}_{13}^{\mathrm{TM}}\rvert^2 \gamma c\sqrt{\varepsilon_{10}/\mu_{10}}}{\omega_p^2 \cos\theta_1 (1+\Re\{\mathcal{Z}_{13}^{\mathrm{TM}}\})}$	$\omega_{\mathrm{opt}}^{\mathrm{TM}} = \frac{\omega_p}{\sqrt{1+\varepsilon_{10}\mu_{21}\Im^2\{\mathcal{Z}_{13}^{*\mathrm{TM}}\}/\cos^2\theta_1}}$ $d_{\mathrm{opt}}^{\mathrm{TM}} = \frac{\cos(\theta_1)c/\sqrt{\varepsilon_{10}\mu_{10}}}{2\omega_{\mathrm{opt}}^{\mathrm{TM}}\mu_{21}\Im\{\mathcal{Z}_{13}^{*\mathrm{TM}}\}} \ln\frac{\varepsilon_{10}(\omega_{\mathrm{opt}}^{\mathrm{TM}})^3 \sin(2/\Im\{\mathcal{Z}_{13}^{*\mathrm{TM}}\})}{\omega_p^2 \gamma \cos(\theta_1)\Im^{-2}\{\mathcal{Z}_{13}^{\mathrm{TM}}\}/4}$
Debye-type: $\sqrt{\frac{\mu_{21}}{\varepsilon_{10}}\left(\varepsilon_h - \frac{\varepsilon_l - \varepsilon_h}{1 - i\omega\tau}\right)}$	$\omega_{\mathrm{opt}}^{\mathrm{TM}} = \frac{2\sqrt{\varepsilon_l\varepsilon_{10}\mu_{21}}(1+\Re\{\mathcal{Z}_{13}\})}{\tau\pi m(\varepsilon_l - \varepsilon_h)\cos^{\mp 1}\theta_1}$ $d_{\mathrm{opt}}^{\mathrm{TM}} = \frac{(\pi m)^2(\varepsilon_l - \varepsilon_h)\tau c/\sqrt{\varepsilon_{10}\mu_{10}}}{2\varepsilon_l\mu_{21}(1+\Re\{\mathcal{Z}_{13}\})\cos^{\mp 1}\theta_1}$	$\omega_{\mathrm{opt}}^{\mathrm{TM}} = \frac{\pi m(\varepsilon_l - \varepsilon_h)\cos^{\mp 1}\theta_1}{2\tau\sqrt{\varepsilon_h\varepsilon_{10}\mu_{21}}(1+\Re\{\mathcal{Z}_{13}\})}$ $d_{\mathrm{opt}}^{\mathrm{TM}} = \frac{2(1+\Re\{\mathcal{Z}_{13}\})\tau c\sqrt{\varepsilon_{10}/\mu_{10}}}{(\varepsilon_l - \varepsilon_h)\cos^{\mp 1}\theta_1}$

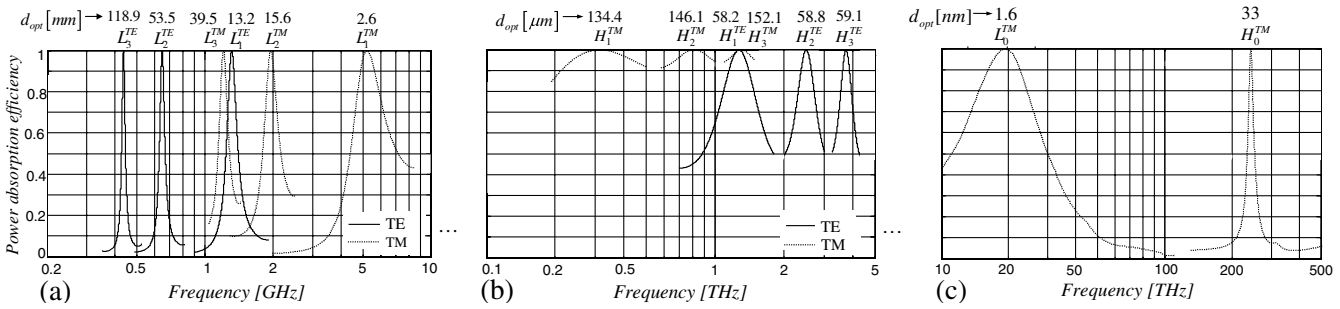

FIG. 3. Broadband absorption spectroscopy (parameter settings as in Fig. 2): (a) Low-frequency intersections ($L_1, \ldots, L_3$) for water layer; (b) High-frequency intersections ($H_1, \ldots, H_3$) for water layer; (c) SPR intersections (L_0^{TM} and H_0^{TM}) for silver layer (TM incidence only).

noted however that, when δ is not sufficiently small, the high-frequency SPR intersection point (H_0^{TM} in Fig. 2) cannot be obtained via (11). This deficiency can be overcome by noting that the SPR mode, obtained above the critical angle, is associated with $r_{23}^{\mathrm{TM}} \to \infty$ [8], leading to $\mathcal{Z}_{12,\mathrm{opt}}^{\mathrm{TM}} \to \mathcal{Z}_{13}^{*\mathrm{TM}} = i\Im\{\mathcal{Z}_{13}^{*\mathrm{TM}}\}$. Furthermore, since in this case (5) is reduced to $\eta = 1 - |R|^2$, optimal power absorption efficiency is readily obtained setting $R = 0$ in (1), resulting in $\varphi_{\mathrm{opt}}^{\mathrm{TM}} = (\psi_{1,\mathrm{opt}}^{\mathrm{TM}} - \psi_{2,\mathrm{opt}}^{\mathrm{TM}})/2 \sim \delta^{\mathrm{TM}} \mathcal{Z}_{12,\mathrm{opt}}^{\mathrm{TM}}$ above and in close vicinity of the critical angle or, explicitly,

$$\mathcal{Z}_{12,\mathrm{opt}}^{\mathrm{TM}} \sim i\Im\{\mathcal{Z}_{13}^{*\mathrm{TM}}\}[1 + 2e^{-2\delta^{\mathrm{TM}}\Im\{\mathcal{Z}_{13}^{*\mathrm{TM}}\} - i2/\Im\{\mathcal{Z}_{13}^{*\mathrm{TM}}\}}]. \quad (15)$$

It should be also noted that above the critical angle, the solution of (7) is identical to the requirement $R = 0$, hence the paths associated with real $\mathcal{Z}_{13}$, which usually terminate [4], become continuous in their transition to the thick slab limit, as depicted in Fig. 2.

Naturally, depending on the particular application, the absorption spectroscopy can be facilitated for any of the three layers involved (Fig. 1). Its potential promise is demonstrated via Fig. 3, where sensitivity of the power absorption efficiency resonance is depicted versus frequency in the vicinity of all the intersection points (resonance frequencies and the associated film thicknesses) in Fig. 2. While the low-frequency intersections of water dispersion with the $m \geq 1$ paths usually occur in the rf and microwave bands [Fig. 3(a)], the high-frequency intersections are expected to occur in the submillimeter and infrared bands [Fig. 3(b)]. One notes that the high-frequency intersection points $H_1, \ldots, H_3$ feature optimal film thicknesses that are almost frequency independent for all the $m \geq 1$ modes [Fig. 3(b) and Table II]. The corresponding metallic film SPR intersections usually occur in the infrared and visible light bands [Fig. 3(c)]. Furthermore, while high-order ($m \geq 1$) paths always intersect perpendicularly the insulator dispersion curves (Fig. 2), these associated with the SPR ($m = 0$) intersect almost tangentially and thus may not intersect at all for incidence angle θ_1 that is too close to the critical angle $\theta_{1,c}$ (when $\Im\{\mathcal{Z}_{13}\}$ becomes too large). Finally, while SPR excitation is impossible below $\theta_{1,c}$, the lossy Fabry-Perot-type modes ($m \geq 1$) can be equally excited also below the critical angle $\theta_{1,c}$ at the cost of lower efficiency.

In summary, highly scalable and sensitive excitation of LRM is possible over a wide range of frequency bands with penetration depths into the absorbing (k_2) and adsorbing (k_3) layers varying from shallow surface-limited sensing to bulk in-depth refractive index measurements.

*Electronic address: danir@tx.technion.ac.il

[1] V. M. Da Costa and L. B. Coleman, Phys. Rev. B **43**, 1903 (1991).
[2] M. Specht, J. D. Pedarnig, W. M. Heckl, and T. W. Hanisch, Phys. Rev. Lett. **68**, 476 (1992).
[3] F. Yang and J. R. Sambles, J. Mod. Opt. **44**, 1155 (1997).
[4] D. Razansky, P. D. Einziger, and D. R. Adam, Phys. Rev. Lett. **93**, 083902 (2004).
[5] B. P. Nelson, A. G. Frutos, J. M. Brockman, and R. M. Corn, Anal. Chem. **71**, 3928 (1999).
[6] I. R. Hooper and J. R. Sambles, J. Appl. Phys. **96**, 3004 (2004).
[7] A. V. Zayats and I. I. Smolyaninov, J. Opt. A Pure Appl. Opt. **5**, S16 (2003).
[8] H. Raether, *Surface Plasmons on Smooth and Rough Surfaces and on Gratings* (Springer, Berlin, 1988).
[9] M. Born and E. Wolf, *Principles of Optics: Electromagnetic Theory of Propagation, Interference and Diffraction of Light* (Cambridge University Press, Cambridge, England, 1999), 7th ed.
[10] C. F. Bohren and D. R. Huffman, *Absorption and Scattering of Light by Small Particles* (Wiley, New York, 1983).
[11] *Handbook of Optical Materials*, edited by M. J. Weber (CRC Press, Boca Raton, 2003).